Probabilistic Optimal Power Flow Incorporating Uncertainties on Load and Renewable Energy Resources

Namami Krishna Sharma[1,*], Rajesh Arya[2], S. C. Choube[3], Akhilesh Kumar Mishra[4], and Rohit Kumar[5]

ARTICLEINFO

Article history:
Received: 14 April 2024
Revised: 3 October 2024
Accepted: 27 November 2011
Online: 15 May 2026

Keywords:
Load uncertainty
Probabilistic optimal power flow
Monte Carlo Simulation
Optimization techniques
Renewable energy sources

ABSTRACT

In the power system, the load uncertainty is comprised of both load and Renewable Energy Resources (RES) and is represented by Probability Density Functions (PDF). Modern power grids are equipped with wind turbines and solar power plants, which combined add unpredictability to the way the power system network operates. The solar irradiance and wind speed follow the beta and Weibull distribution respectively, are the main sources of electricity for wind turbine generators and solar PV systems. However, power system load, which has a normal distribution, is an important factor contributing to the power system's uncertainty. This work proposes the Probabilistic Optimal Power Flow (POPF) method and investigates the impact of load uncertainty on the power system's functionality and the optimal state of power system operation. In response to the uncertain set of input data (electrical load, wind velocity, solar irradiance), the uncertainty in terms of PDF for slack bus power generation is evaluated using Monte Carlo Simulation (MCS) in this work. The objective function in the proposed work utilizes a curated function of the minimization of the normalized sum of voltage deviation magnitudes, real power loss, and L-index (Bus). Normalization assures equal weightage for all three parts of the objective function. Following the identification of a critical scenario, the power flow has been optimized utilizing the Rao-1 optimization technique to ensure optimal performance of the power system. The outcomes were subsequently compared with those obtained through the utilization of the Jaya and black-hole optimization methods. The developed methodology has been successfully executed on the 26-bus system and provides superior performance. The system under investigation operates 8.21% better with the JAYA optimization algorithm that of BHA, further performance significantly improves with utilizing Rao-1 by 21.8% that of JAYA. The result shows the supremacy of the proposed approach.

Nomenclature

P_{Dk}	MW loading at k^{th} load bus.
Q_{Dk}	MVAR loading at k^{th} load bus.
μ_1	Location parameter in MW (mean value of uncertain MW loadings)
σ_1	Scale parameter in MW (standard deviation of uncertain MW loadings)
μ_2	Location parameter in MVAR (mean value of uncertain MVAR loadings)
σ_2	Scale parameter in MVAR (standard deviation of uncertain MVAR loadings)
Ψ_N	Input uncertainty following normal distribution.
$[m \times n]$	$[48 \times 1]$.
$P_{k\,net}$	Net active power in MW atk^{th}load bus after incorporation of DG units.
$Q_{k\,net}$	Net reactive power in MW at k^{th}load bus after incorporation of DG units.
$P_{WTG\,k}$	Power output in MW from WTG unit connected at k^{th} load bus.
$Q_{WTG\,k}$	Reactive power drawn in MVAR by conventional WTG unit connected at k^{th} load bus
$P_{solar\,k}$	Power output in MW from solar/PV unit at k^{th}load bus.
A	Scale parameter at given location in the unit of wind speed
K	Shape parameter at a given location (dimensionless)
v	Velocity of wind in m/s.
ρ_a	Air density 1.225 kg/m^3
C_P	0.5926 (Turbine coefficient)

[1]*Department of Electrical Engineering, Prestige Institute of Engineering Management and Research, Indore, India.*
[2]*Computer Science and Engineering Department, Sushila Devi Bansal College of Engineering, Indore, India.*
[3]*Department of Electrical & Electronics engineering, University Institute of Technology(UIT), RGPV, Bhopal, India.*
[4]*Department of EEE, IILM University, Greater Noida, India.*
[5]*Department of Electrical Engineering, Govt. Polytechnic Jamui, Kalyanpur Road, Jamui, India.*
**Corresponding author:* Namami Krishna Sharma; Email: er.namami@gmail.com.

A'	Cross-sectional area of wind turbine in m^2 (radius=70m)
Φ	WTG power factor angle
v_{cut-in}	3.5m/s (Cut-in velocity)
v_{cutout}	20m/s (Cut-out velocity of wind)
v_{rated}	11m/s (Rated wind velocity)
P_{inet}	Net MW at i^{th} bus
P_{Di}	MW demand at i^{th} bus
P_{PV}	MW supplied by Solar PV unit
a & b	Shape parameters having values 4 and 2.
H	Average solar irradiation (KW/m^2).
E	Energy (kWh).
A''	Total area of solar panel (158 m^2).
r	Yield ratio of Solar Panel (14%).
PR	Performance ratio (0.75).
$x_i(t)$	i^{th} star location at t^{th} iteration
x_{BH}	Black hole in the search space.
R	Event horizon radius
f_{BH}	Fitness value
f_i	Fitness value of i^{th} star
i	Current iteration number
j	No. of design variables
k'	Population size
$X_{j,k',i}$	j^{th} variable of k'^{th} candidate in i^{th} iteration.
r_1 & r_2	Random variables ranging from (0-1).
F	Overall objective function
F_1	Sum of absolute values of voltage deviations at load buses associated with output uncertainty ξ
F_2	Total real power losses in MW
V_k^{ξ}	k^{th} bus voltage sample associated with output uncertainty ξ
ξ	Represents Uncertainty returns to output variables due to input uncertainty Ψ_N
k	Set of load buses.
P_{Li}	i^{th}transmission line loss.
F_1^0	Value of F_1 for base case condition (before optimization).
F_2^0	Total transmission line losses before optimization.
F_3	Maximum value of L_index for a bus.
F_3^0	Maximum value of F_3 before optimization.
P_{Gi}^{ξ}	MW generation at i^{th} bus associated with output uncertainty ξ
P_{Di}^{ψ}	MW demand at i^{th} bus associated with input uncertainty ψ
$P'_{DG\,i}$	Injected MW by DG units at i^{th} bus
Q_{Gi}^{ξ}	MVAR generation at i^{th} bus associated with output uncertainty ξ
Q_{Di}^{ψ}	MW demand at i^{th} bus associated with input uncertainty ψ
$Q'_{DG\,i}$	MVAR drawn at i^{th} bus DG units
$P_i(V^{\xi}\ \delta^{\xi})$	Net MW at i^{th} bus as function of voltage and its angle contains output uncertainty ξ on them
$Q_i(V^{\xi}\ \delta^{\xi})$	Net MVAR at i^{th} bus as function of voltage and its angle contains output uncertainty ξ on them
V_i	Voltage magnitude at i^{th} bus
Ψ	Input uncertainty factor
$Q_{sh,i}$	Reactive compensation in MW at i^{th} bus
L_index_k	Lindex of k^{th} load bus
β_L	Set of load or PQ buses
β_G	Set of generator or PV buses
F_{ki}	Subset of the hybrid matrix
L_{ij}	L-index of line connected between bus i and j
X_{ij},R_{ij}	Reactance and resistance of the line connected between bus i and j in ohms

1. INTRODUCTION

With the growing prevalence of green energy (wind and solar), it is imperative for system operators to effectively address its stochastic properties in a manner that is both dependable and cost-effective. It is possible to resolve the trade-off between competing goals by considering the variability and uncertainty of solar and wind power generation. Most of the research on power systems only considers deterministic situations, failing to account for what happens when input parameters vary or are randomly selected. This research examines the effect of load uncertainty on the operation of the power system. The paper highlights the noteworthy contribution of the uncertainty handling process towards achieving optimal operation of power systems. Electric power systems encompass a multitude of uncertain parameters with varying degrees of diversity. The proper treatment and management of indeterminate variables is a crucial aspect. A. Rezaee Jordehi outlines the sources of uncertainties that are present in power systems in [1]. Article [1] also comprehensively classified and reviewed various methods for handling uncertainty in power systems. For the power system to operate optimally, uncertainties must be accurately estimated, modelled, and represented. The categorization of probabilistic methods, as presented in Fig. 1 (b), for addressing uncertainties in power systems is classified into three primary groups. In order to address the uncertainties associated with load flow analysis, a probabilistic method called Monte-Carlo simulation is commonly utilized. In order to assess the applicability of these three distinct and efficient estimation techniques—point estimation methods, an analytical cumulant-based approach, and the probabilistic collocation method—in probabilistic small disturbance stability analysis of large uncertain power systems, this article compares them [2]. Contemporary advancements in technology to the operation and analysis of power systems, encompassing novel and significant domains are addressed in [3]. Optimal power flow strategies along with uncertainty analysis are deeply explained in [3]. The researchers in [4] explore the dynamic characteristics of operation in relation to a standard voltage/power curve. Y. Dvorkin *et. al.* in [5] introduces a novel approach for determining uncertainty sets pertaining to the parameters of probability distributions. The variability of wind velocity contributes to the uncertainty of distributed generation. The Weibull distribution is utilized to model the wind flow. Globally, nations are incorporating photovoltaic power generation systems into their electrical grids as a means of bolstering their efforts to combat climate change.

Solar power generation is subject to significant uncertainty as a result of fluctuations in solar irradiance levels throughout the day. Inaccurate modelling of this fluctuation could lead to inefficient use of system resources. Accurate solar irradiance pattern characterisation is essential for effective renewable energy resource management in an electrical power system. System control plays an important role in mitigating oscillations in system variables, but is rarely taken into consideration by traditional PLF approaches [6]. The planning of electrical power system expansion using probabilistic load flow (PLF) techniques is described in [7]. In article [8], the correlations between random variables are examined and the available PLF techniques in distribution networks are reviewed and categorized. Additionally, a thorough comparison of different uncertainty modeling approaches is presented, with their correctness, complexity, and simulation time evaluated. Two new Probabilistic Load Flow (PLF) approaches that are based on the holomorphic embedding method and are intended to manage uncertainties and integrate renewable energy in power networks are discussed in [9]. Because of the substantial uncertainty added by the growing usage of electric vehicle (EV) charging and photovoltaic (PV) generation in distribution grids, probabilistic load flow (PLF) approaches are necessary for more precise analysis. PLF consists of three main parts: PLF computations, correlation models, and probability distribution models [10].

This work presents a systematic probabilistic approach to guarantee optimal power system operation in the presence of uncertainty. Ensuring the electricity system operates optimally in the face of uncertainty is the aim of this research.

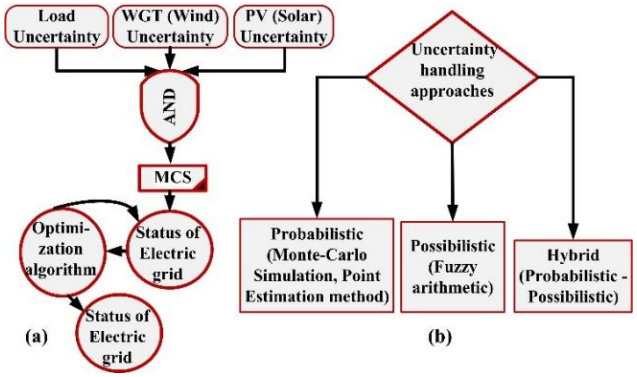

Fig. 1. (a) Uncertainty handling process, and (b) Methodology for uncertainty.

This study examines how power system operations are impacted by uncertainty arising from renewable energy sources and power system demands. Uncertain modelling has been developed for both loads and renewable energy resources. Subsequently, the models characterized by their inherent uncertainty are incorporated into a power system network comprising 26 buses. In the context of probabilistic optimal power flow, the output variable's probability distribution function (PDF) is found by applying the Monte-Carlo simulation (MCS) technique, which effectively manages the dependencies among the inputs. The system exhibits a level of imprecision in the output parameters, considering the uncertainties in the input. The present approach involves a specific collection of output parameters of a system that are subject to uncertainties in the input. The proposed methodology can be comprehensively grasped by referring to Fig. 2. Performance indices, in particular the Minimum Eigenvalue of load flow Jacobian, have been utilized to identify the criticality of the system or its critical operating condition in light of the numerous uncertainties [11].

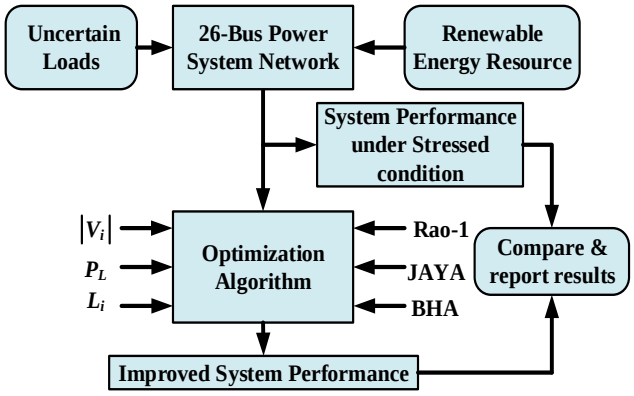

Fig. 2. Block diagram of optimal probabilistic power flow.

An indicator denoted as $'L'$ exhibits variability within the numerical interval of 0 (representing the absence of system load) and 1(voltage collapse) is developed by P. Kessel *et al.* in [12]. Another index that assesses the stability of lines is developed in [13]. The present research utilizes a comparative analysis of the Rao-1, JAYA, and Black Hole optimization algorithms in the context of conducting an optimal power flow investigation. The methodology depicted in Fig. 1 (a) could potentially be utilized to conduct uncertainty analysis.

The following are the main contributions of the suggested work:

- The integration of power system demands and Renewable Energy Resources (RES) as sources of uncertainty in the system is the main focus of the study.
- This study focuses on the development of models for uncertain load and renewable energy sources (RES) utilizing Normal, Weibull, and Beta distributions.
- The application of Monte-Carlo simulation in the conversion of probabilistic problems into

deterministic ones is a topic of interest.

- The utilization of contemporary optimization methodologies such as Rao-1, Jaya, and BHA is employed to attain the optimal operational state in the presence of system uncertainties.

The presented work has been organized into 7 sections. Section 2 describes the process of creating models for loads that are subject to uncertainty. Section 3 defines the construction of models for distributed generation that incorporate uncertainty. Section 4 establishes algorithms for optimization techniques. Section 5 presents a methodology for conducting uncertainty analysis through the utilization of Monte-Carlo simulation (MCS). Section 6 presents results and discussion and lastly, Section 7 presents conclusions.

2. UNCERTAIN ELECTRICAL LOAD MODEL

The data about the 26-bus system has been sourced from reference [11]. The introduction of uncertainty in the behavior of electrical loads necessitates the utilization of Normally distributed models, wherein the mean value corresponds to the base load. The modelling of uncertain load model based on normal distribution at selected buses is presented in reference [3]. Load uncertainties have been accounted via modelling and this gives information of worst-case load flow results i.e. voltage profile.

The general formula for the normal distribution's probability density function with uncertain loads at the k^{th} bus is:

$$f(\mathrm{P_{Dk}}) = \frac{e^{\frac{(\mathrm{P_{Dk}}-\mu_1)^2}{2\sigma_1^2}}}{\sigma_1\sqrt{2\Pi}} \quad (1)$$

$$\mathrm{P_{Dk}}(\Psi_N) = \mathrm{normrnd}(\mu_1, \sigma_1, \mathrm{m}, \mathrm{n}) \quad (2)$$

$$\mathrm{f(Q_{Dk})} = \frac{e^{\frac{(\mathrm{Q_{Dk}}-\mu_2)^2}{2\sigma_2^2}}}{\sigma_2\sqrt{2\Pi}} \quad (3)$$

$$\mathrm{Q_{Dk}}(\Psi_N) = \mathrm{normrnd}(\mu_2, \sigma_2, \mathrm{m}, \mathrm{n}) \quad \text{and } \sigma > 0 \quad (4)$$

3. DISTRIBUTED GENERATION MODELING

3.1. Wind Turbine Generator Model

The correlation between the electrical power of WTG/Solar and electrical loads can be addressed as a net load concept:

$$\mathrm{P_{k\,net}} = \mathrm{P_{WTG\,k}}/\mathrm{P_{solar\,k}} - \mathrm{P_{Dk}} \quad (5)$$

$$\mathrm{Q_{k\,net}} = \mathrm{Q_{WTG\,k}} + \mathrm{Q_{Dk}} \quad (6)$$

where, $\mathrm{P_{solar\,k}}$ - is power output in MW from solar/PV unit at k^{th}load bus.

The modeling of wind turbine generators (WTG) regarding wind uncertainty is explicated in reference [5]. The wind flow adheres to the Weibull distribution in the following manner.

$$\{v\ (\Psi_W) = wblrnd(K, A, [m, n]) \quad (7)$$

Ψ_W = input uncertainty following Weibull distribution.

'K' varied from 1.0 to 3.0 and 'A' varied from 5 to 20 taken from [14].

The electrical output of WTG depends on wind velocity and the performance characteristic of the generator is obtained using the following equations:

$$\mathrm{P_{WTG\,K}} = \begin{cases} \frac{1}{2}\rho_a A' v^3 C_p & ;\ \mathrm{v_{cutin}} \le \mathrm{v} \le \mathrm{v_{rated}} \\ 7.136\ \mathrm{MW} & ;\ \mathrm{v_{rated}} \le \mathrm{v} \le \mathrm{v_{cutout}} \end{cases} \quad (8)$$

$$\mathrm{Q_{WTG\,K}} = \mathrm{P_{WTG\,k}}\mathrm{Tan}\Phi \quad (9)$$

where, (Cos Φ = 0.75 lagging).

3.2. Solar PV modeling

The generation of electrical power through a Solar/PV unit is primarily contingent upon solar irradiance, as evidenced by sources [6]. In [15], a novel energy-based performance ratio (PR) is presented as a standard for evaluating the EE of big solar installations. The electrical power output of solar energy is dependent on solar irradiation, which is typically described by the Beta distribution function, as stated below:

$$\{H\ (\Psi_B) = betarnd(c, d, [m, n]).* 100 \quad (10)$$

Ψ_B = input uncertainty following Beta distribution.

The electrical energy generated by a solar PV system:

$$\mathrm{E} = \mathrm{A''} \times \mathrm{r} \times \mathrm{H} \times \mathrm{PR} \quad (11)$$

Hourly electrical power output of the Solar PV unit can be simulated by hourly average solar irradiation using equation (12). The irradiance variation is taken from the reference [15].

$$\mathrm{P_{PV}} = \frac{\mathrm{A''} \times \mathrm{r} \times \mathrm{H} \times 10^{-6}}{24}\ \mathrm{MW} \quad (12)$$

Net load at bus *i*:

$$\mathrm{P_{inet}} = \mathrm{P_{Di}} - \mathrm{P_{PV}} \quad (13)$$

The steps for integrating the sources of uncertainty into Probabilistic Optimal Power Flow (POPF) are as follows:

a. Development of a dynamic load flow program: This dynamic load flow program receives load information, solar irradiance, and wind flow information as input data.

b. These input data are modelled using probability density functions (Section 2 and Section 3).

Once the load uncertainties are evaluated, they are incorporated into the POPF model as input parameters. Finding the optimal operating point that minimizes the objective function while meeting the constraints and taking the unknown load state into account is the goal of the POPF analysis. Further, Section 4 presents the utilized optimization algorithms in the proposed work. Risk of

uncertainties in renewable sources can be accounted by simulation and may be mitigated by improving failure rate and repair time of each component of renewable energy sources or modifying the network. The details of this study form our future agenda of research. This study will require not only simulation but optimization also in different formulation.

4. MODERN OPTIMIZATION TECHNIQUES

4.1. Black Hole Algorithm 'BHA'

One technique for population-based optimisation is the Black Hole Algorithm [16]. One way to formulize "star absorption" is:

$$x_i(t+1) = x_i(t) + \mathrm{rand}\left(x_{BH} - x_i(t)\right) \quad (14)$$

where:

$x_i(t)$ - i^{th} star location at t^{th}iteration.

x_{BH} - black hole in the search space.

Event horizon radius 'R' is formulated as follows:

$$R = \frac{f_{BH}}{\sum_{i=1}^{N} f_i} \quad (15)$$

The fitness value of the black hole and i^{th} star is represented by f_{BH} and fi respectively. When the candidate solution or the star is approaching the event horizon of a black hole or best particle. The distance between the candidate solution and the best candidate is calculated by equation (15).

The black hole's and the i^{th} star's fitness values are denoted by f_{BH} and f_i respectively. when the best particle or the candidate solution approaches the black hole's or star's event horizon. Equation (15) computes the distance between the candidate solution and the best candidate.

4.2. JAYA optimization algorithm

The Sanskrit word JAYA means "Victory." This is a simple and effective optimisation method based on the idea that the current solution steers towards the optimal solution while avoiding the worst one. R. V. Rao created this method in [17]. The following is the candidate position update equation and common control parameters:

$$X_{j,k',i}^{updated} = X_{j,k',i} + r_{1,j,i}\left(X_{j,best,i} - \left|X_{j,k',i}\right|\right) - r_{2,j,i}\left(X_{j,worst,i} - \left|X_{j,k',i}\right|\right) \quad (16)$$

where:

i - current iteration number

j - no. of design variables

k' - population size,

$X_{j,k',i}$ - j^{th} variable for k'^{th} candidate at i^{th} iteration.

r_1 and r_2 are the random variables ranging from (0-1).

In the event that the updated position of the candidate outperforms the current position corresponding to $X_{j,k',i}^{current}$, the updated position of the candidate replaces the current position; otherwise, the candidate's previous position is maintained throughout the process until the termination criterion is met.

4.3. Rao-1 optimization algorithm

The algorithm for optimization has been elaborated upon in reference [18]. An Improved Rao-1 (IRao-1) algorithm is presented in Article [19], which improves global search capability without sacrificing simplicity. According to experimental data, IRao-1 works more accurately and efficiently than recent algorithms for a range of PV models. The operational concept involves utilizing the candidate's past optimal and suboptimal values within the exploration area to update its current position. This is achieved through the application of the subsequent equation.

$$X_{j,k',i}^{updated} = X_{j,k',i}^{current} + r_{1,j,i}\left(X_{j,best,i} - X_{j,worst,i}\right) \quad (17)$$

The candidate's updated position replaces the current position if the solution corresponding to $X_{j,k',i}^{updated}$ is superior to that corresponding to $X_{j,k',i}^{current}$ otherwise, the candidate's previous position is kept. This process is repeated until the termination criterion is met.

5. METHODOLOGY AND PROBLEM FORMULATION

5.1. Monte-Carlo simulation

The utilization of a probabilistic approach is an effective method for addressing parametric uncertainty issues. Monte Carlo simulation (MCS) is a technique that can be employed to enhance the efficacy of this approach. MCS operates based on probability density function (PDF) distributions at input parameters and subsequently determines the unknown PDFs at output parameters [20]. Article [21] discusses a modified approach to power flow analysis, transitioning from static state to multi-period analysis using the MATPOWER program. The diagram depicting MCS can be observed in Fig. 3 which shows that MCS takes uncertain input parameters and under the presence of design variables and system constraints it provides output. The power system's input-output relationship can be expressed as:

$$Z = f(X, Y) \quad (18)$$

Uncertainty in input variables is represented by X and Y is the set of decision variable parameters of the system. MCS yields the output value of Z by utilizing the input-output correlation for every given set of input PDFs. The probability density function that offers the best fit to the output variables is used to represent the variable Z. The findings derived from the Monte Carlo simulation (MCS)

are further elaborated in section 6.2 of this paper. Monte Carlo simulation is the only methodology to deal uncertainties in the system. Analytical techniques cannot deal with large number of uncertainties present in the systems.

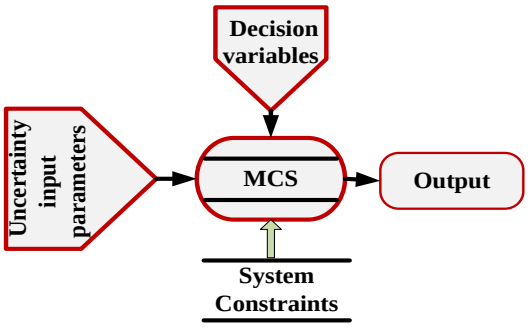

Fig. 3. Monte-Carlo Simulation.

5.2. Problem formulation

Finding the power system's optimal operational state is the primary goal of the proposed effort. After converting the problem from a probabilistic to a deterministic one the objectives required for optimal operation of power system are developed in this section. Three operational objectives are important in the formulation of the overall objective function i.e.

(i) Bus voltage deviation from nominal voltage of 1.0 pu.

(ii) Real power loss in transmission line

(iii) Voltage stability consideration

As a result, the objective function selected is the minimization of the normalized sum of voltage deviation magnitudes, real power loss and L-index (Bus). Normalization assures equal weightage to all three parts of the objective function. Hence the function '*F*' is written as:

$$F = \frac{F_1}{F_1^0} + \frac{F_2}{F_2^0} + \frac{F_3}{F_3^0} \quad (19)$$

Objective function = min (F) (19a)

$'F'$ comprises from normalized values of $'F_1'$ $'F_2'$ and $'F_3'$. These sub-objective functions are defined as follows:

$$F_1 = \sum_k \left(\text{abs} \left(1 - V_k^{\xi} \right) \right) \quad (20)$$

$'F_1'$ is the magnitude of voltage deviation at all the load buses. V_k^{ξ} indicates k^{th} bus voltage value associated with output uncertainty ξ:

$$F_2 = \sum P_{Li} \quad (21)$$

$'F_2'$ MW loss in the group.

$$F_3 = \max [L\_index_k] \quad (22)$$

$'F_3'$ indicates the L_index value of bus 'k', which is highest amongst the other L_index (bus) values. The operating point's proximity to the voltage collapse point is indicated by the value of the L_index. L-index (bus) value is unity at voltage collapse point. L-index is very low for unloaded condition and reaches unity at voltage collapse points. Therefore, as seen by the PV-curve in Figure 4, its size indicates how close the current operating point is to the collapse point. Article [22] presents an optimization technique for addressing voltage sags in power distribution systems through the integration of photovoltaic (PV) energy generation.

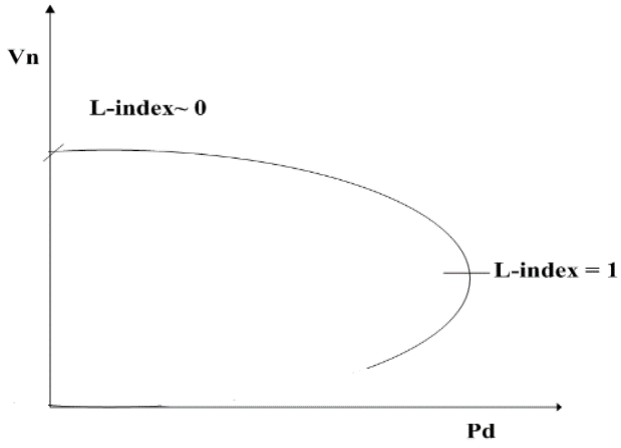

Fig. 4. PV- Curve.

Since voltage magnitude alone does not indicate how close the operating point is to the collapse point, voltage stability consideration is crucial. Hence in addition to 'F_1' 'F_3' has been considered. Need not be stressed that loss minimization is an important issue from an efficiency viewpoint. The following constraints apply to the minimisation of the objective function represented by equation (19):

(i) Power flow equation containing the effects of input and output uncertainties are the first equality constraint of our problem.

$$P_{Gi}^{\xi} - P_{Di}^{\Psi} + P'_{DG\,i} = P_i(V^{\xi}, \delta^{\xi}) \quad (23)$$

$$Q_{Gi}^{\xi} - Q_{Di}^{\Psi} - Q'_{DG\,i} = Q_i(V^{\xi}, \delta^{\xi}) \quad (24)$$

(ii) Bus voltage values are treated as inequality constraints

$$V_{min,i} \leq V_i \leq V_{max,i} \quad (25)$$

(iii) While developing the model for input uncertainties various limiting factors like shape parameters, standard deviation, and mean values are combined the part of the input uncertainty factor and can be represented as follows:

$$\Psi_{min} \leq \Psi \leq \Psi_{max} \quad (26)$$

(iv) Range of shunt compensation to be provided at selected buses is another inequality constraint:

$$Q_{sh,i}^{min} \leq Q_{sh,i} \leq Q_{sh,i}^{max} \quad (27)$$

The values for L_index (bus) and L_index (line) have been determined using the following equations:

L_index (Bus):

$$L\_index_k = \max_{k \in \beta_L} \left| 1 - \frac{\sum_{i \in \beta_G} F_{ki} V_i}{V_k} \right| \quad (28)$$

L_index (line):

$$L_{ij} = \frac{4\left[(P_j X_{ij} - Q_j R_{ij})^2 + (P_j R_{ij} + Q_j X_{ij}) V_i^2\right]}{V_i^4} \quad (29)$$

6. RESULTS AND DISCUSSION

6.1. Selection of distribution generation units under base case condition of 26-bus system

A flowchart illustrating the steps involved in addressing a restricted optimisation issue is shown in Fig. 5. The power system is comprising 26 buses, of which 6 are designated as generator buses, and a total of 46 lines are present, as documented in Appendix A and reference [11]. Table 1 presents the L_index (line) values for the base cases that were computed utilizing equation (29) to determine the distribution generation placement as given in Table 1. The 15th line is linked to buses 6 and 19, which exhibit the highest L_index value. These two load buses have thus been recognised as viable candidates for the WTGs units. In the same manner, it can be observed that line number 6 establishes a connection between buses 2 and 13, with the latter possessing the second-largest L_index. Consequently, only bus number 13 has been identified as a potential candidate for the installation of a Solar/PV unit, as bus number 2 is already designated as a PV bus. Fig. 6 displays the power output curve of a solar/PV unit, this curve is obtained by putting appropriate values in equation (8) discussed in section 3.1. From cut-in to rated velocity the wind power output follows a rising trend and after obtaining the rated speed the real power output of WTG becomes constant as represented in Fig. 6.

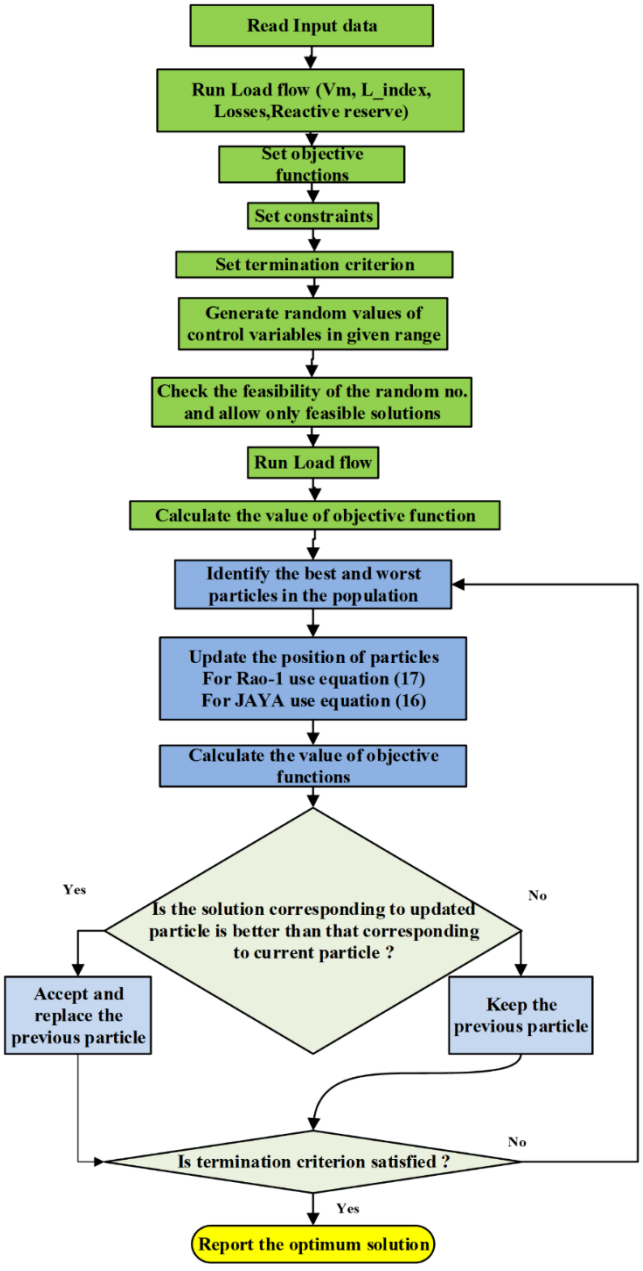

Fig. 5. Flowchart of the proposed methodology.

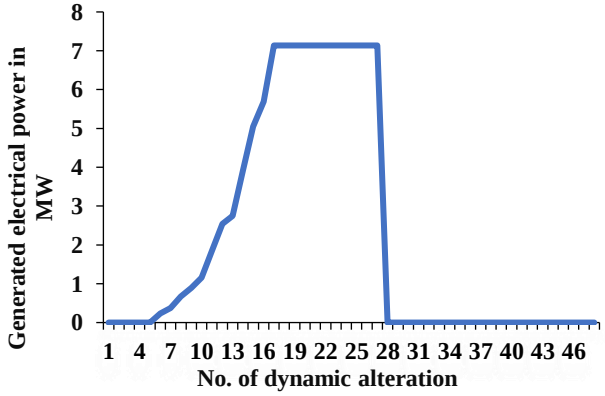

Fig. 6. Electric power generation supplied by WTG.

Table 1. Base case condition of the 26-bus system.

Line no.	L_Index (line)	Line no.	L_Index (line)	Line no.	L_Index (line)
1	0.0184	17	0.0129	33	0.0358
2	0.0643	18	0.1513	34	0.0227
3	0.0985	19	0.0155	35	0.0104
4	0.0973	20	0.0746	36	0.0927
5	0.0854	21	0.0170	37	0.0424
6	**0.1769**	22	0.0539	38	0.1019
7	0.0182	23	0.0342	39	0.1312
8	0.0158	24	0.0456	40	0.1122
9	0.0127	25	0.0823	41	0.0126
10	0.0278	26	0.0800	42	0.0119
11	0.1589	27	0.0324	43	0.0353
12	0.0192	28	0.0027	44	0.0073
13	0.0085	29	0.0522	45	0.0388
14	0.0379	30	0.0845	46	0.0099
15	**0.1831**	31	0.1170	**L_index (line)**	
16	0.0755	32	0.0349		

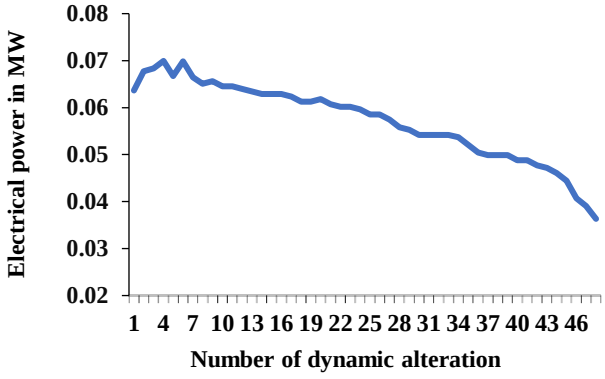

Fig. 7. Electric power generation supplied by the PV-Solar.

Similarly, the output MW curve of a solar PV unit is depicted in Fig. 7. This output is obtained by putting appropriate values in equation (12) and equation (8) discussed in section 3.2.

6.2. Uncertainty analysis using Monte-Carlo Simulation

The generation of uncertainty in output variables has been accomplished through the utilization of MCS, as elucidated in sub-section 5.1. As a result of the aforementioned uncertainties, the computation of the slack bus power generation's variation and its corresponding probabilistic distribution are displayed, respectively, in Figs. 8 and 9. The aim is to determine the most appropriate probability density function (PDF) for the acquired values of power generation at the slack bus. Fig. 10 presents the most appropriate probability density function for the actual power generation of the slack bus. Table 2 presents parametric values corresponding to various probability distributions on slack bus real power.

Table 2. Parametric values for different distributions on slack bus real power

Name of distribution	Parametric values	
Normal	μ=1117.7 [1082.9, 1152.66]	σ=120.136 [100.01, 150.48]
Weibull	A = 1171.17 [1138.94, 1204.3]	K = 10.7187 [8.59092, 13.3734]
Gamma	a = 87.009 [58.364, 129.713]	b = 12.8467 [8.60743, 19.1739]
Kernel	Kernel = normal	Bandwidth = 69.0006
Exponential	μ=1117.78 [858.454, 1516]	

Real power generation at slack bus corresponding to dynamic alterations of input values is depicted in Fig. 8. Its probabilistic curve is shown in Fig. 9 and best best-suited PDF curve is shown in Fig. 10.

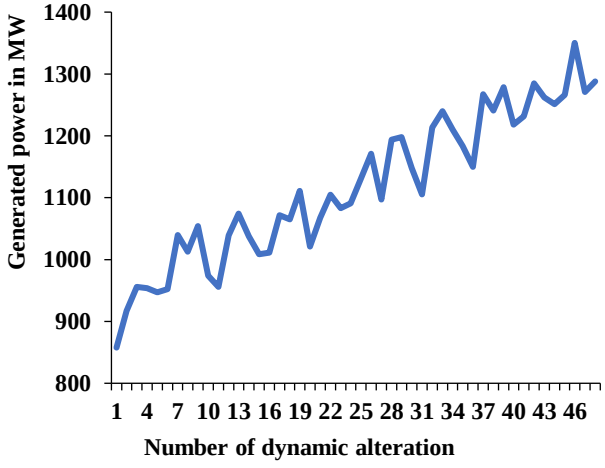

Fig. 8. Slack bus power generation in MW.

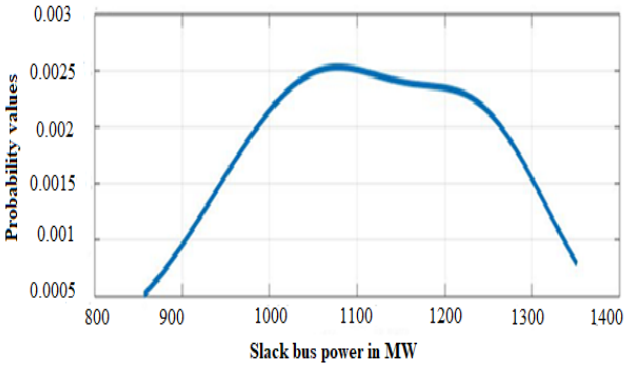

Fig. 9. Probability distribution of slack bus Power generation.

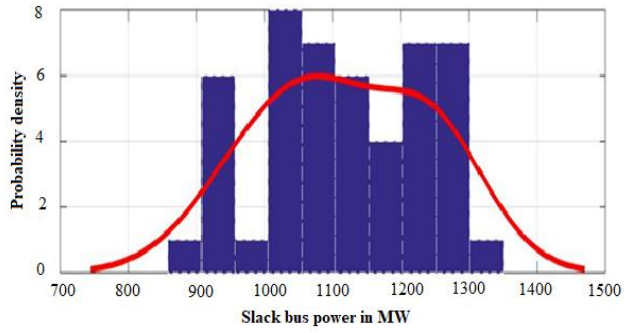

Fig. 10. Best-suited PDF on real power generation of Slack bus.

The power system experiences diverse operational modifications due to input parametric uncertainties. The operator needs to take precautions against the worst-case scenario in order to guarantee the best possible operation of power systems in the face of uncertainty. To determine the critical case, the system utilizes various indices such as the P-V curve, Q-V curve, Line index, FVSI, or minimum eigenvalue of load flow. One technique for showing the current operating conditions of a power system is the Jacobian matrix, which is used in the Newton-Raphson load flow approach. The load flow's minimal eigenvalue The Jacobian matrix serves as a gauge for the system's overall criticality, whereas Lindex is an indicator to check the criticality of a bus or a line. Lindex lies between 0 and 1. All lines and buses offer different Lindex values between 0 and 1, but the whole system offers only one lowest eigenvalue of the power flow Jacobian matrix for any one set of input values. That is why the authors have used the power flow Jacobian index to identify critical operating states and the Lindex to place WTG units. Fig. 11 depicts the fluctuation of the lowest eigenvalue of the power flow Jacobian matrix about the input uncertainties. We have designed our input uncertainty modelling in such a manner that it could produce 48 different values with defined PDF functions on it. Corresponding to these input values the power system offers different behaviors for each input alteration. To find out the most critical case corresponding to input alteration we have used lowest eigenvalue of the power flow Jacobian matrix as an indicator. The variation of lowest eigenvalue of the power flow Jacobian matrix corresponding to input alteration is depicted in Fig. 11. Where we can observe that minimum value encountered is 2.7899 corresponding 46th alteration of input. Now set of input data corresponding to 46th case is selected as main input data for critical case load flow analysis. Now our aim is to improve the system characteristics corresponding to the critical case, through optimal reactive compensation with the help of Rao-1 optimization algorithm, which is discussed in section 6.3.

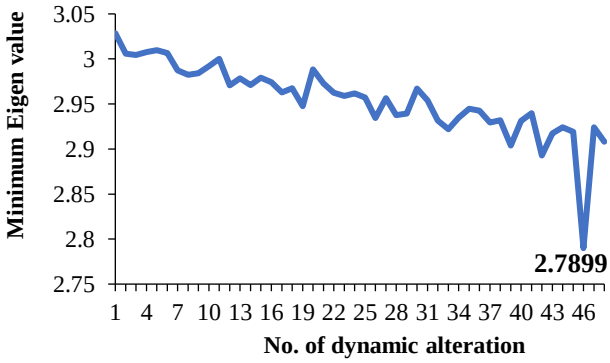

Fig. 11. Variation of lowest eigenvalue of the power flow Jacobian.

6.3. Simulation results and discussion

The assumed limits for load bus voltages are 0.95pu-1.05pu. Table 3 displays the load on the bus, bus voltages, and the value of L_index (bus) during a simulated stressed condition. Fig. 12 illustrates the $L\_index\ (bus)$ of all PQ-buses, as determined by relation no. (28). The selection of shunt compensation placement is determined by identifying the PQ-bus with the highest L_index (bus) value. The optimization algorithm generated initial populations (m) of 100 for each of the seven design variables, specifically chosen for the placement of shunt compensation, namely $Qsh\_17, Qsh\_19, Qsh\_21, Qsh\_22, Qsh\_23, Qsh\_24,$ and Qsh_25. The generation process was conducted randomly of shunt compensation ranging from 0.00 to 20 MVAR, as previously reported in [11]. The N-R power flow analysis was conducted while considering all inequality constraints (23) – (27) for various sets of randomly generated design variables, to identify the optimal and suboptimal solutions. The simulation procedure was halted after 23 iterations as a result of the convergence of the fitness function solution. The load bus voltage of the most vulnerable or important load buses under stress is shown in Fig. 13, both before and after the shunt compensation is placed. The shunt compensation has been optimized using the Rao-1 technique, and the results have been compared with those obtained using the Jaya and BH techniques. A comparison of the locations of shunt compensation at the most vulnerable load buses is displayed in Fig. 14 using Rao-1 with other well-established optimization techniques such as

Jaya and BH techniques. Fig. 15 depicts a graph that illustrates a comparison of the objective function through the utilization of Rao-1, Jaya, and BH techniques. A graph comparing the convergence of the total objective function with the number of iterations is shown in Fig. 16. The findings indicate that the Rao-1 algorithm superior to the Jaya and BH optimization techniques in terms of achieving better global optimal results.

Fig. 12 shows the bus index values of 26 bus test systems bus no. 13 having the lowest value i.e., 0.0166, and bus no. 24 having the highest value of L-index i.e., 0.2463. From Fig. 4 one can observe that a lower value of L_index means the system is operating under healthy conditions and a higher value (near to 1) of L_index means that the bus is operating near its stability limit. Based on this discussion we can identify the critical or candidate buses for the placement of reactive compensation to improve the operation of the system. Each optimization technique provides the optimal value of compensation for candidate buses.

After the optimal reactive support is provided to the system, the increment in bus voltage values be seen in Fig. 13. The comparison of load bus voltages is shown in Fig. 13, with four vertical graphs in different colors for each load bus voltage. The load bus voltage for the critical case is shown in blue (without optimization or optimal compensation), and the remaining three colors are load bus voltages that were obtained using optimization techniques (with optimal compensation). Before the implementation of optimization outcomes, bus 24 exhibited a minimal voltage value of 0.7854 per unit (pu). After the application of optimization results, the bus voltage attains a value of approximately 1.00 pu, as depicted in Fig. 13. Rao-1 provides better results as compared to other optimization techniques.

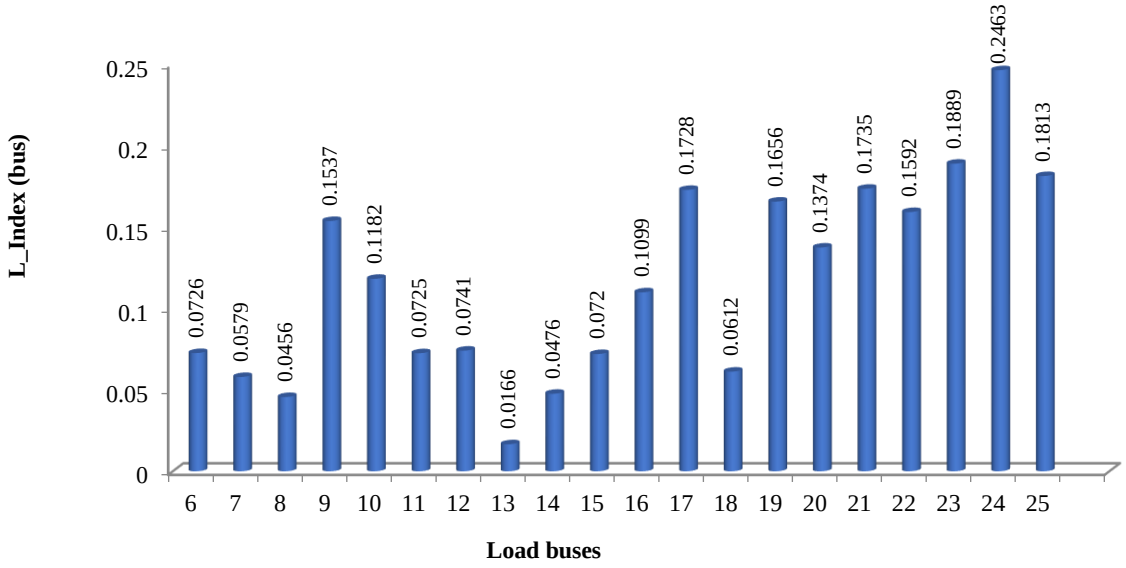

Fig. 12. L_index (bus) of load buses for 26-bus system.

Table 3. Stressed case results

Bus no.	$\|V_m\|$ (pu)	δ in degree	P_G (pu)	Q_G (pu)	L_index (bus)	P_D (pu)	Q_D (pu)
1	1.0250	0	13.526	6.312	-	0.51	0.41
2	1.0100	-1.72	0.79	0.932	-	0.22	0.15
3	1.0250	-6.81	0.20	1.369	-	0.64	0.50
4	1.0000	-7.13	1.00	0.448	-	0.25	0.10
5	1.0150	-1.55	3.00	1.557	-	0.50	0.30
6	0.9934	-5.42	0	0	0.0726	0.76	0.29
7	0.9494	-6.29	0	0	0.0579	0.00	0
8	0.9536	-6.35	0	0	0.0456	0.00	0
9	0.9352	-11.2	0	0	0.1537	2.18713	1.22872
10	0.9019	-10.2	0	0	0.1182	0.00	0.00
11	0.9778	-6.02	0	0	0.0725	0.24699	0.27927
12	0.9422	-8.76	0	0	0.0741	1.76106	0.94979

13	0.9998	-7.20	0	0	0.0166	0.27856	0.15
14	0.9780	-8.42	0	0	0.0476	0.23389	0.02854
15	0.9629	-9.28	0	0	0.0720	0.73596	0.17857
16	0.8738	-10.2	0	0	0.1099	0.67472	0.24108
17	0.8554	-10.0	0	0	**0.1728**	1.76745	0.75191
18	0.9826	-3.66	0	0	0.0612	3.02745	1.32574
19	0.9037	-11.0	0	0	**0.1656**	0.75	0.15
20	0.9242	-10.9	0	0	0.1374	0.59394	0.27213
21	0.8621	-11.0	0	0	**0.1735**	0.68701	0.25135
22	0.8567	-11.6	0	0	**0.1592**	0.52469	0.21373
23	0.8276	-12.3	0	0	**0.1889**	0.35675	0.12811
24	0.7854	-14.2	0	0	**0.2463**	1.27532	0.63766
25	0.8877	-11.5	0	0	**0.1813**	0.30755	0.09537
26	0.9934	-3.97	0.60	0.477	-	0.40	0.20
Total		P_G=19.11677		Q_G=11.09786		P_D=18.6828	Q_D=8.83189

In Fig. 14 the results obtained from the Rao-1 technique are also dominating over other optimization techniques. Fig. 14 shows the requirement of total shunt compensation in MVAR at candidate buses to ensure the optimal operation of power system. Fig. 15 shows the optimised value of the objective function equation (19a). A formulation of the optimisation problem to minimise the objective function was made in Section 5.2. The objective function attains a minimum value of 30.0983, as determined by the Rao-1 algorithm. This finding underscores the efficacy of the Rao-1 algorithm relative to other optimization techniques in addressing similar problems. Fig. 16 illustrates the convergence properties of each optimization method. The Rao-1 method requires a greater number of iterations; however, it yields superior outcomes.

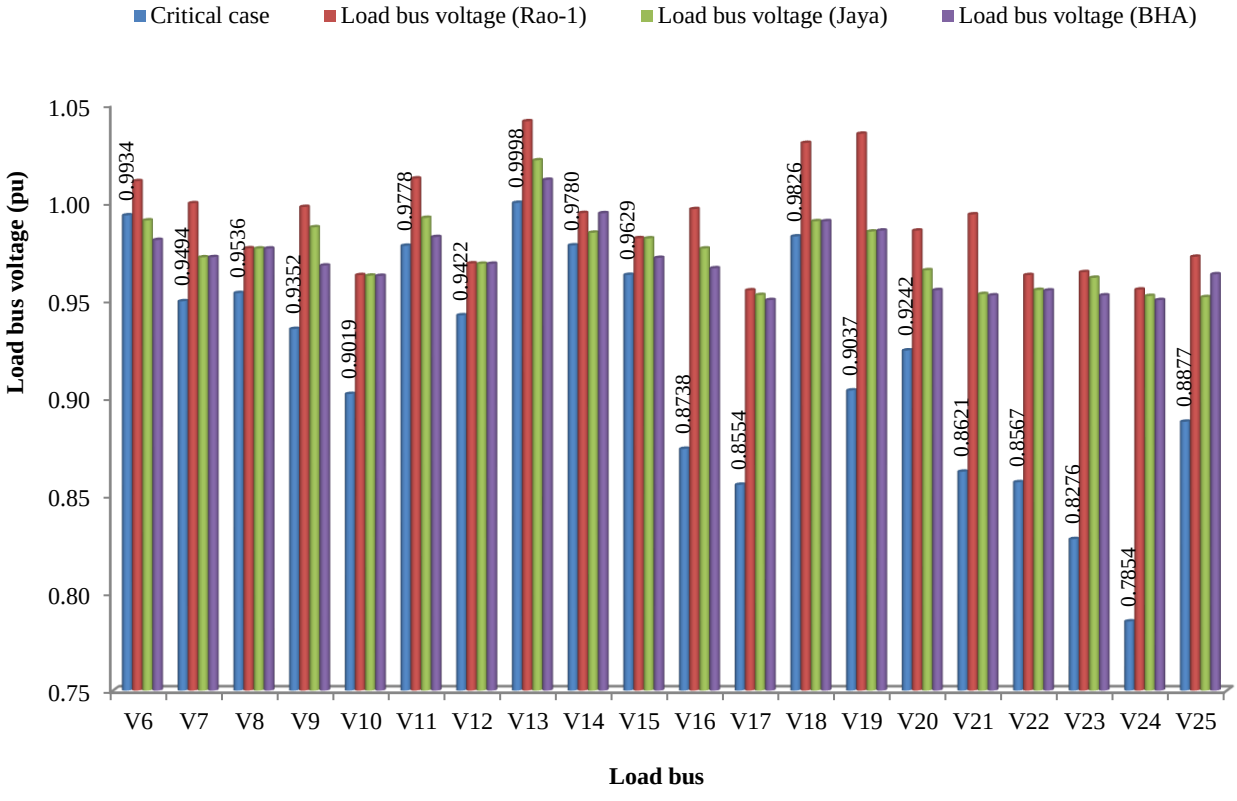

Fig. 13. Comparison of Load bus voltages without and with optimization techniques for 26-bus test system.

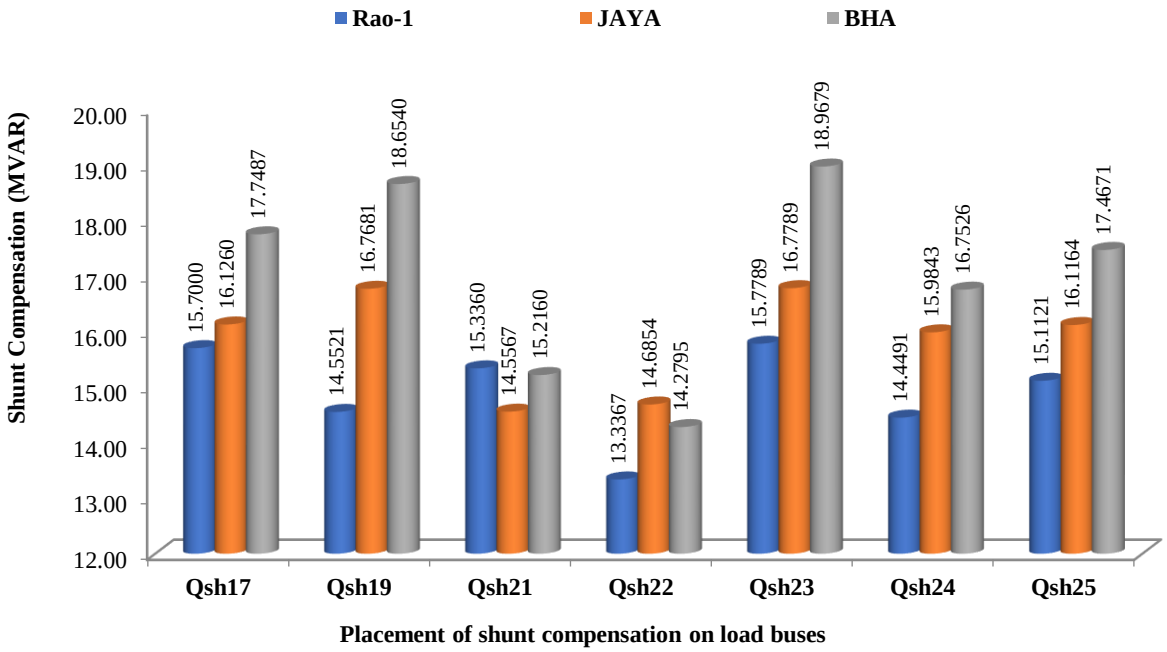

Fig. 14. Comparison of optimal placement of shunt compensation at most sensitive load buses (bus no. 17, 19, 21, 22, 23, 24 & 25) using Rao-1, Jaya, and BH for 26-bus test system.

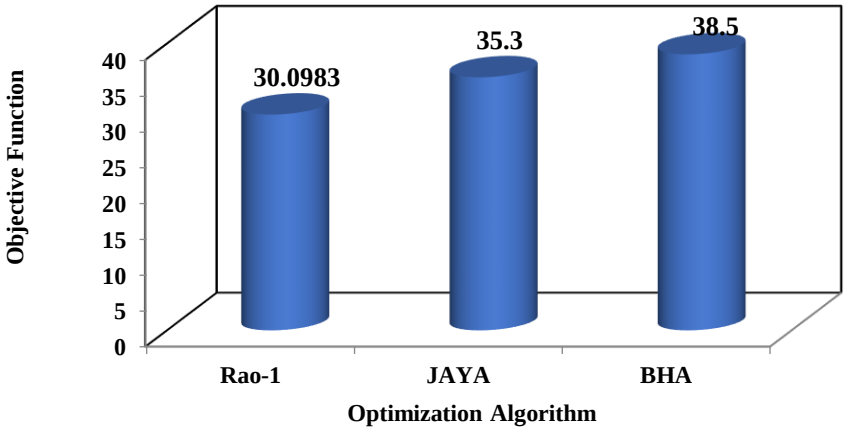

Fig. 15. Comparison of the objective function using Rao-1, Jaya, and BH for 26-bus test system.

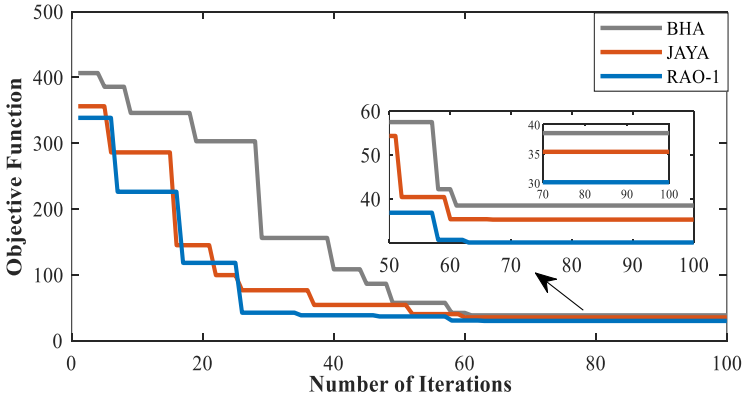

Fig. 16. Comparative convergence curve.

This study employs probability function-based uncertain modeling, Monte Carlo simulation, and a well-established optimization technique to determine the optimal operational state under conditions of uncertainty. The objective function has been improved by 8.31% concerning BHA utilizing JAYA, further, this has been enhanced by 21.84% with the proposed algorithm (RAO-1).

7. CONCLUSION

The present work proposes a novel probabilistic methodology for predicting the optimal power flow, by considering uncertainties in loads and distributed generations while adhering to stability constraints. In this study, 48 segments have been identified to carry out the necessary study throughout 24 hours. Further sets of state variables have been extracted from distributed generation and uncertain load models. A probabilistic load flow analysis program has made use of the sets as input parameters. The impact of input uncertainty has been investigated by utilising Monte-Carlo Simulation (MCS) to produce the probability distribution of the output variables. Once a constrained optimization issue was identified, the system's simulated stressed condition within the given uncertainties was determined. The normalised total of the voltage deviation magnitudes, real power loss, and voltage stability factors was the goal of this optimisation task. To guarantee the power system operates as efficiently as possible, this has been done. The feasibility of the suggested approach has been exhibited through the application of the methodology on a 26-bus standard test system utilizing the 'Rao-1' optimization technique. The resulting outcomes have been compared with those obtained from the 'JAYA' and 'Black Hole Algorithm' optimization techniques. The system under investigation now operates 8.21% better with the JAYA optimization algorithm that of BHA, further performance significantly improves with utilizing Rao-1 by 21.8% that of JAYA. The result shows the supremacy of the proposed approach.

Appendix-A [11]
Data for 26-Bus system (100 MVA Base)

Table A-1: Line data

Line No.	Bus No.		Resistance (pu)	Reactance (pu)	Susceptance (pu)	Tap
	From	To				
1	1	2	0.0005	0.0048	0.0300	1.000
2	1	18	0.0013	0.0110	0.0600	1.000
3	2	3	0.0014	0.0513	0.0500	0.960
4	2	7	0.0103	0.0586	0.0180	1.000
5	2	8	0.0074	0.0321	0.0390	1.000
6	2	13	0.0007	0.0054	0.0005	0.960
7	2	26	0.0323	0.1967	0.0000	1.000
8	3	13	0.0007	0.0054	0.0005	1.017
9	4	8	0.0008	0.0240	0.0001	1.050
10	4	12	0.0016	0.0207	0.0150	1.050
11	5	6	0.0069	0.0300	0.0990	1.000
12	6	7	0.0053	0.0306	0.0010	1.000
13	6	11	0.0097	0.0570	0.0001	1.000
14	6	18	0.0037	0.0222	0.0012	1.000
15	6	19	0.0035	0.0660	0.0450	0.950
16	6	21	0.0050	0.0900	0.0226	1.000
17	7	8	0.0012	0.0069	0.0001	1.000
18	7	9	0.0009	0.0429	0.0250	0.950
19	8	12	0.0020	0.0180	0.0200	1.000
20	9	10	0.0010	0.0493	0.0010	1.000
21	10	12	0.0024	0.0132	0.0100	1.000

22	10	19	0.0547	0.2360	0.0000	1.000
23	10	20	0.0066	0.0160	0.0010	1.000
24	10	22	0.0069	0.0298	0.0050	1.000
25	11	25	0.0960	0.2700	0.0100	1.000
26	11	26	0.0165	0.0970	0.0040	1.000
27	12	14	0.0327	0.0802	0.0000	1.000
28	12	15	0.0180	0.0598	0.0000	1.000
29	13	14	0.0046	0.0271	0.0010	1.000
30	13	15	0.0116	0.0610	0.0000	1.000
31	13	16	0.0179	0.0888	0.0010	1.000
32	14	15	0.0069	0.0382	0.0000	1.000
33	15	16	0.0209	0.0512	0.0000	1.000
34	16	17	0.0990	0.0600	0.0000	1.000
35	16	20	0.0239	0.0585	0.0000	1.000
36	17	18	0.0032	0.0600	0.0380	1.000
37	17	21	0.2290	0.4450	0.0000	1.000
38	19	23	0.0300	0.1310	0.0000	1.000
39	19	24	0.0300	0.1250	0.0002	1.000
40	19	25	0.1190	0.2249	0.0004	1.000
41	20	21	0.0657	0.1570	0.0000	1.000
42	20	22	0.0150	0.0366	0.0000	1.000
43	21	24	0.0476	0.1510	0.0000	1.000
44	22	23	0.0290	0.0990	0.0000	1.000
45	22	24	0.0310	0.0880	0.0000	1.000
46	23	25	0.0987	0.1168	0.0000	1.000

Table A-2: Bus Data

Bus No.	**Voltage (pu)**	**Load**		**Generation**		**Reactive power limits**		**Shunt compensation**
		Pd (MW)	**Qd (MVAR)**)	**Pg (MW)**	**Qg (MVAR)**	**Q_{min} (MVAR)**	**Q_{max} (MVAR)**	**Q_{sh} (MVAR)**
1	1.025	51.000	41.000	0.000	0.000	0.000	0.000	0.000
2	1.020	22.000	15.000	79.000	0.000	40.000	250.000	0.000
3	1.025	64.000	50.000	20.000	0.000	40.000	150.000	0.000
4	1.050	25.000	10.000	100.00	0.000	40.000	80.000	0.000
5	1.045	50.000	30.000	300.00	0.000	40.000	160.000	0.000
6	1.000	76.000	29.000	0.000	0.000	0.000	0.000	0.000
7	1.000	0.000	0.000	0.000	0.000	0.000	0.000	0.000
8	1.000	0.000	0.000	0.000	0.000	0.000	0.000	0.000
9	1.000	89.000	50.000	0.000	0.000	0.000	0.000	0.000
10	1.000	0.000	0.000	0.000	0.000	0.000	0.000	0.000
11	1.000	25.000	15.000	0.000	0.000	0.000	0.000	0.000
12	1.000	89.000	48.000	0.000	0.000	0.000	0.000	0.000
13	1.000	31.000	15.000	0.000	0.000	0.000	0.000	0.000
14	1.000	24.000	12.000	0.000	0.000	0.000	0.000	0.000

15	1.000	70.000	31.000	0.000	0.000	0.000	0.000	0.000
16	1.000	55.000	27.000	0.000	0.000	0.000	0.000	0.000
17	1.000	78.000	38.000	0.000	0.000	0.000	0.000	0.000
18	1.000	153.000	67.000	0.000	0.000	0.000	0.000	0.000
19	1.000	75.000	15.000	0.000	0.000	0.000	0.000	0.000
20	1.000	48.000	27.000	0.000	0.000	0.000	0.000	0.000
21	1.000	46.000	23.000	0.000	0.000	0.000	0.000	0.000
22	1.000	45.000	22.000	0.000	0.000	0.000	0.000	0.000
23	1.000	25.000	12.000	0.000	0.000	0.000	0.000	0.000
24	1.000	54.000	27.000	0.000	0.000	0.000	0.000	0.000
25	1.000	28.000	13.000	0.000	0.000	0.000	0.000	0.000
26	1.015	40.000	20.00	60.000	0.000	15.000	50.000	0.000

REFERENCES

[1] Rezaee Jordehi, A. 2018. How to deal with uncertainties in electric power systems? A review. Renewable and Sustainable Energy Reviews 96: 145–155.

[2] Preece, R.; Huang, K; Milanović, J.V. 2014. Probabilistic Small-Disturbance Stability Assessment of Uncertain Power Systems Using Efficient Estimation Methods. IEEE Transactions on Power Systems 29 (5): 2509-2517.

[3] Zhu, J. 2015. Optimization of Power System Operation. New Jersey: John Wiley & Sons.

[4] Rajagopalan, C.; Lesieutre, B.C.; Sauer, P.W.; Pai, M.A. 1992. Dynamic aspects of voltage/power characteristics. IEEE Transaction on Power System 7: 990–1000.

[5] Dvorkin, Y.; Lubin, M.; Backhaus, S.; Chertkov, M. 2016. Uncertainty Sets for Wind Power Generation. IEEE Transactions on Power Systems 31 (4): 3326-3327.

[6] Jia, M.; Cao, Q.; Shen, C.; Hug, G. 2023. Frequency-Control-Aware Probabilistic Load Flow: An Analytical Method. IEEE Transactions on Power Systems 38 (6): 5170-5187.

[7] Leite da Silva, A.M.; Ribeiro, M.P.; Arienti, V.L.; Allan, R.N.; Do Coutto Filho, M.B. 1990. Probabilistic Load Flow Techniques Applied to Power System Expansion Planning. IEEE Transactions on Power Systems 5: 1047-1053.

[8] Abbasi, A.R.; Mohammadi, M. 2023. Probabilistic load flow in distribution networks: An updated and comprehensive review with a new classification proposal. Electric Power Systems Research 222.

[9] Abbasi, A.R. 2020. Probabilistic Load Flow Based on Holomorphic Embedding, Kernel Density Estimator and Saddle Point Approximation Including Correlated Uncertainty Variables. Electric Power Systems Research 183.

[10] Ramadhani, U.H.; Shepero, M.; Munkhammar, J.; Widén, J; Etherden, N. 2020. Review of probabilistic load flow approaches for power distribution systems with photovoltaic generation and electric vehicle charging. International Journal of Electrical Power & Energy Systems 120.

[11] Hadi, S. 1999. Power System Analysis. New York: McGraw-Hill.

[12] Kessel, Glavitsch, H. 1986. Estimating the Voltage Stability of a Power System. IEEE Transactions on Power Delivery 1 (3): 346-354.

[13] Jasmon, G.B.; Lee, L.H.C.C. 1991. Distribution Network Reduction for Voltage Stability Analysis and Load Flow Calculations. International Journal of Electrical Power and Energy Systems 13(1): 9-13.

[14] Hetzer, J.; Yu, D.C.; Bhattarai, K. 2008. An Economic Dispatch Model Incorporating Wind Power. IEEE Transactions on Energy Conversion 23(2): 603-611.

[15] Jamil, I.; Lucheng, H.; Habib, S.; Aurangzeb, M.; Ahmed, E.M.; Jamil, R. 2023. Performance evaluation of solar power plants for excess energy based on energy production. Energy Reports 9: 1501-1534.

[16] Hatamlou A. 2013. Blackhole: A new heuristic optimization approach for data clustering. Information Sciences Elsevier 222: 175–184.

[17] Rao, R.V. 2016. Jaya: A simple and new optimization algorithm for solving constrained and unconstrained optimization problems. International Journal of Industrial Engineering Computations 7: 19–34.

[18] Rao, R.V. 2020. Rao algorithms: Three metaphor-less simple algorithms for solving optimization problems. International Journal of Industrial Engineering Computations 11: 107-130.

[19] Farah, A.; Benabdallah, F.; Belazi, A.; Almalaq, A.; Chtourou, M.; Abido, M.A. 2022. An improved Rao-1 algorithm for parameter estimation of photovoltaic models 260.

[20] Zou, B.; Xiao, Q. 2014. Solving Probabilistic Optimal Power Flow Problem Using Quasi-Monte Carlo Method and Ninth-Order Polynomial Normal Transformation. IEEE Transactions on Power Systems 29 (1): 300-306.

[21] Noppanut, C.; Pongsuk, P.; Yuttan, K.; Rungphet, K.; Krittidet, B.; Kaan, K. 2025. Modified MATPOWER for Multi-Period Power Flow Analysis with PV Integration. GMSARN International Journal 19: 165-174.

[22] Papon N.; Nattachote, R. 2024. Optimization Technique for Voltage Sag with Integration of Photovoltaic Energy Distributed Generation. GMSARN International Journal 18: 414-420.